J Nanostruct 15(3): 1075-1084, Summer 2025

RESEARCH PAPER

Studying Structural and Optical Properties of ZnO and Ag NPs Produced by Laser-Induced Plasma in liquid technique (PLAL) for Antibacterial Applications

Hassan H. Lafta *, Ahmed K. Abbas

Department of Physics, College of Science, University of Wasit, Al-kut, Iraq

ARTICLE INFO

Article History:
Received 05 March 2025
Accepted 24 June 2025
Published 01 July 2025

Keywords:
Ag nanostructures
Colloid solution
Laser energy, PLAL
Laser induced plasma

ABSTRACT

The aim of this work was to examine the optical properties and structure of metal and metal oxide nanostructures. The pulsed laser ablation in liquid technique (PLAL) was used to produced colloidal solutions of silver and ZnO nanostructures with median energies 500mJ to 700mJ and the same frequency of 6Hz were prepared by using a Nd/YAG laser system with wavelength at 1064 nm. A crystalline structure and shape was shown by (XRD) pattern, which included many nanostructure peaks at different energies. Crystalline sizes were found to be (7.99-21.43) nm of the samples (ZnO) and (7.36-38.04) nm of samples Ag. .Field emission scanning electron microscopy (FE-SEM) images showed the appearance of nanostructures and their regular aggregation and the cubic - shape of Silver(Ag) , Grain clusters shape and homogeneous distribution of ZnO nanostructures .Additionally, absorbance spectra covering a range of wavelengths from 200 - 1100 nm were used to examine each colloidal solution optical characteristics Band gap energy E_g values in the optical properties decreased with increasing laser intensity, dropping within the ranges of 3.09 to 2.77 eV of ZnO and 5.54 to 5.04 eV of Ag . The antibacterial activity of ZnO and Ag nanoparticles was evaluated with two types of bacteria (Escherichia coli and Staphylococcus *aureus*) using the liquid method. the activity of ZnO NPs is found against E. coli at (18-23) mm and against S.aureus at (18-20)mm.The activity of Ag is found against E.coli at (21-22.5) mm, and against S. aureus at (19-21) mm by using 500mJ 700mJ, respectively.

How to cite this article
Lafta H., Abbas A. Studying Structural and Optical Properties of ZnO and Ag NPs Produced by Laser-Induced Plasma in liquid technique (PLAL) for Antibacterial Applications. J Nanostruct, 2025; 15(3):1075-1084. DOI: 10.22052/JNS.2025.03.024

INTRODUCTION

in recent years, the Use of ultrafast lasers for micro- and nanomanufacturing has grown in popularity and become rapidly growing worldwide industry. The ability of laser machining to work within liquid environments, which attempts to improve control over quality of surface and efficiency of ablation, is also another reason contributing to its increasing appeal. Among the several advantages of using a liquid medium, including minimizing the amount of heat that reaches the targets and producing clean surfaces. Consequently, laser ablation in liquids (PLAL) has become popular for a variety of uses, including laser printing and cleaning [1].

In PLAL, as opposed to typical laser machining, where the target surface is the primary output, the final product is the scattered materials that

* *Corresponding Author Email: Std2023204.hshujair@uowasit.edu.iq*

arise from ablation in the liquid.

The surface of the resultant nanoparticles typically experiences chemical changes during PLAL, leading to the creation of defects such as oxidized noble metal NP surfaces or NPs affected by oxygen vacancies [2]. By applying laser energy to a target in a liquid medium, the complex process of laser ablation in a liquid environment removes metal with selectivity [3,4]. The numerous steps involved in this action are depicted in Fig.1. First, the laser pulse is absorbed by the metal, causing it to rapidly heat up before vaporizing.

The vaporization process creates plasma, which quickly expands to produce shock waves that move through the liquid medium. High-pressure liquid streams directed at the metal surface are created when cavitation bubbles created by these shock waves eventually burst. These high-pressure liquid streams strike the metal, causing it to fracture and ablate, removing material from the target.

There are several factors that affect how well laser ablation works in a liquid medium. such as the laser's energy, wavelength, pulse length, liquid media, and the metal substrate's inherent

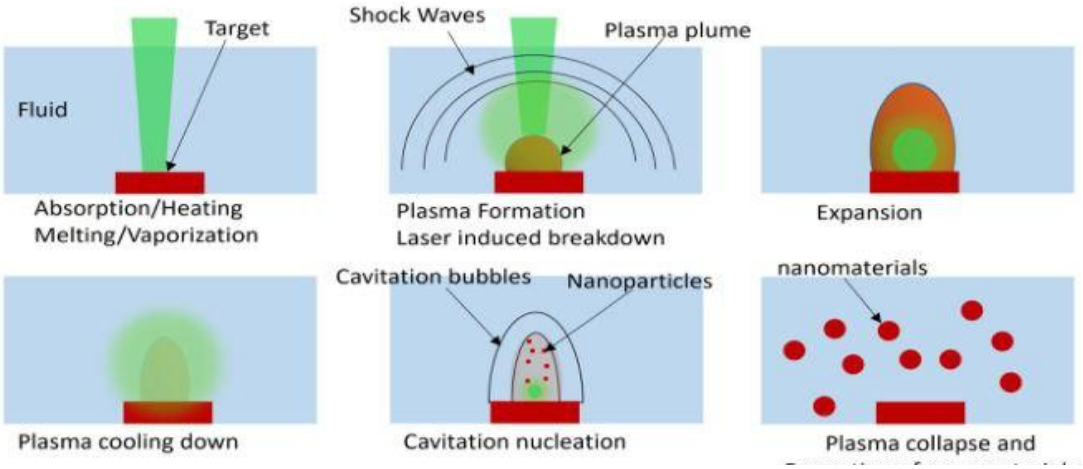

Fig. 1. Schematic illustration of the laser ablation during the laser-target-liquid system.

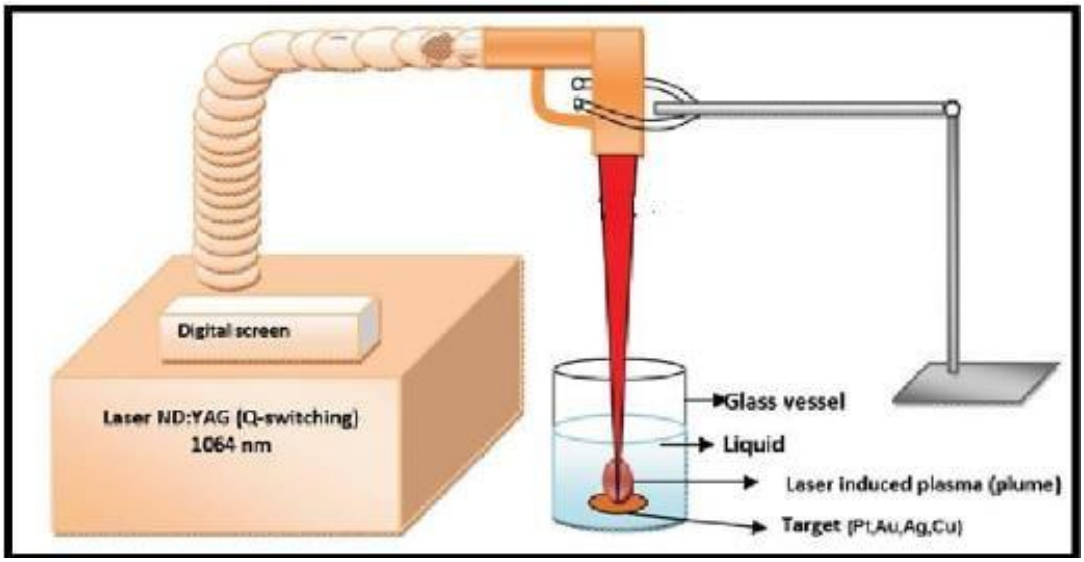

Fig. 2. PLAL system using Nd:YAG with wavelength 1064nm.

properties. By maximizing these factors, material removal can be carried out accurately and efficiently with the least amount of affect to the surrounding material [5] (PLAL) technique, which combines between top-down method and bottom-up method processes, is frequently recognized as a hybrid approach physic [3]

MATERIALS AND METHODS

Silver and Zinc plates (1cm x1cm) with thickness of 2mm and more than 99.99% pure was used (XiAN company.China). The target immersed at 9mm depth in 3 milliliters of distilled deionized water in glass beaker with volume 5 mL. Laser ablation was performed by a (Nd:YAG)laser with 1064 nm Q-switched system type HUAFEL and higher intensity: 2000 mJ/pulse, time of pulse: 10 nanosecond, the rate of repletion: (10 Hz), diameter of the beam: (5 mm) and focal length of 10 mm are seen in Fig. 2. Materials and tools of test antibacterial activity are shown in Table 1.

The preparation of Muller-Hinton (M-H) Agar

It was made by mixing 38 g of the powder M-H with 1 L of distilled water, then heating it on a stove while shaking. To sanitize M-H, autoclave it for 15 minutes at 121°C. The mixture was then allowed to cool to 50 °C before being poured into a petri dish, left for about 15 minutes to solidify, turned upside down, and refrigerated at 4 °C.

RESULTS AND DISCUSSION

X-ray Diffraction analysis (XRD)

X-ray diffraction analysis of both [Silver (Ag), ZnO] nanostructures prepared by using different laser energy (500-700) mJ are shown in Fig. 3. The

Table 1. Materials and tools are used for test antibacterial activity.

Materials and tools	Com.	Origin(country)
balance 4 digits	hangzhou	China
round Flask	Labmaxn	Germany
hot plate Magnetic stirrer	four E's	China
incubator	ningbo	Chain
autoclave	westtlne	Chain
glass erlenmeyer flask	pyrex	Germany
Ethanol	Duksan	Korea
Mueller Hinton agar	accumix	Spin

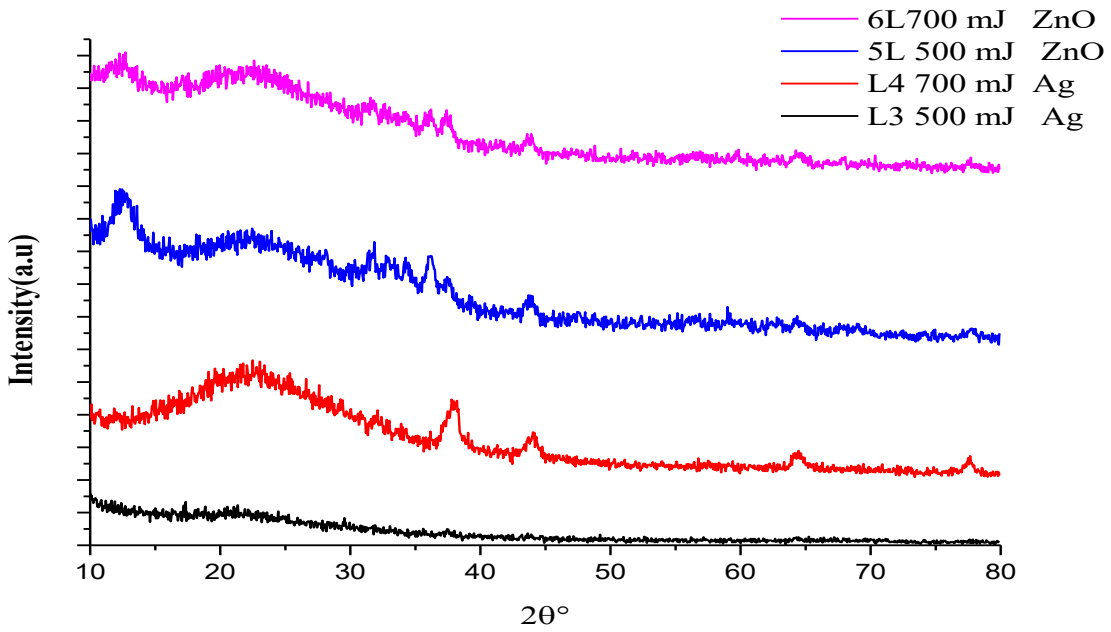

Fig. 3. XRD Patterns of Ag nanostructures.

Table 3. The Activity of NPs (Ag ,ZnO).

			B		
E(mJ)	2θ (Deg.)	FWHM (Deg.)	Crystallite size (nm)	Average Crystallite size (nm)	hkl
700mJ	38.25	0.42	19.98	22.19	(111)
	43.71	1.00	8.54		(200)
	64.58	0.25	38.04		((202)
500 mJ	37.81	1.14	7.36	9.05	(111)
	43.94	1.03	8.31		(200)
	64.48	0.93	10.09		(202)
	77.64	0.98	10.45		(311)
			A		
E mJ	2θ (Deg.)	FWHM (Deg.)	Crystallite size (nm)	Average Crystallite size (nm)	hkl
500 mJ	31.63	0.59	13.99	14.51	100
	36.14	0.56	14.92		022
	43.73	0.97	8.82		101
	59.05	0.45	20.29		012
700 mJ	31.54	0.68	12.14	13.06	100
	36.12	0.39	21.43		022
	37.36	1.05	7.99		101
	43.72	0.80	10.70		012

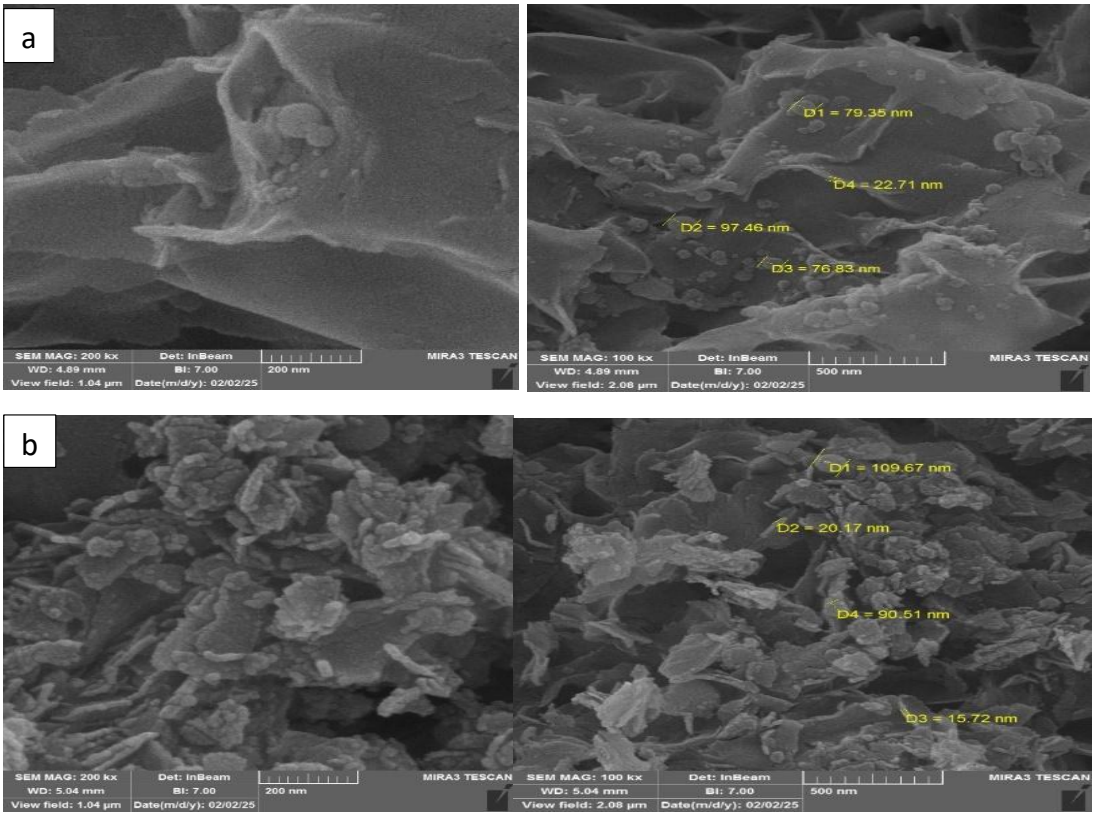

Fig. 4. FE-SEM images and length distribution of ZnO NPs at range (200nm and 500 nm) with laser energy (a) 500mJ and (b) 700Mj.

polycrystalline cubic of Ag and hexagonal structures of ZnO in all matched those on the (No·96-110-0137) and (No. 96-230-0451) respectively. As seen in Fig. 3, the lattice planes (100), (022), (101), and (012) were indicated by many peaks at diffraction angles (2θ) of 31.63, 36.14, 43.73, and 59.05, respectively for ZnO nanostructures.

The XRD pattern of Ag samples showed peaks at angles of diffraction (2θ): 38.03, 43.83, 64.41, and 77.64, which correspond to the lattice planes : (111), (200), (202), and (311), respectively.

peak positions changed as laser energy increased because the lattice uniform strain varied with crystalline sizes, in were observed [6]. Additionally, It is evident that as laser energy increased, peak intensity increased while peak width reduced, indicating to crystalline size and higher crystallinity·

At the same laser energy, ZnO nanostructures gave a greater XRD peak intensity than the Ag nanostructures, there is smaller interaction between the target and the laser beam at Zinc Oxide because of decreasing absorption by the surface. So Zinc Oxide absorbs less photons, which allows more energy to create the X-ray diffraction signals and increase the peak intensity· The size of each individual crystal (D) in a polycrystalline film was determined by Scherer's equation[7]:

$$D = \frac{k\lambda}{\beta\cos(\theta)} \quad (1)$$

θ is The Bragg angle, ß is the full breadth at half maximum by radians, λ is wavelength of X-ray, k is constant and equal 0.94.. The diffraction characteristics for ZnO and Ag thin films created with different laser energy are shown in Table1.

Field Emission Scanning Electron Microscopy (FE-SEM)

The surface morphology of ZnO and Ag nanoparticles is shown in Figs. 4 and 5. Because

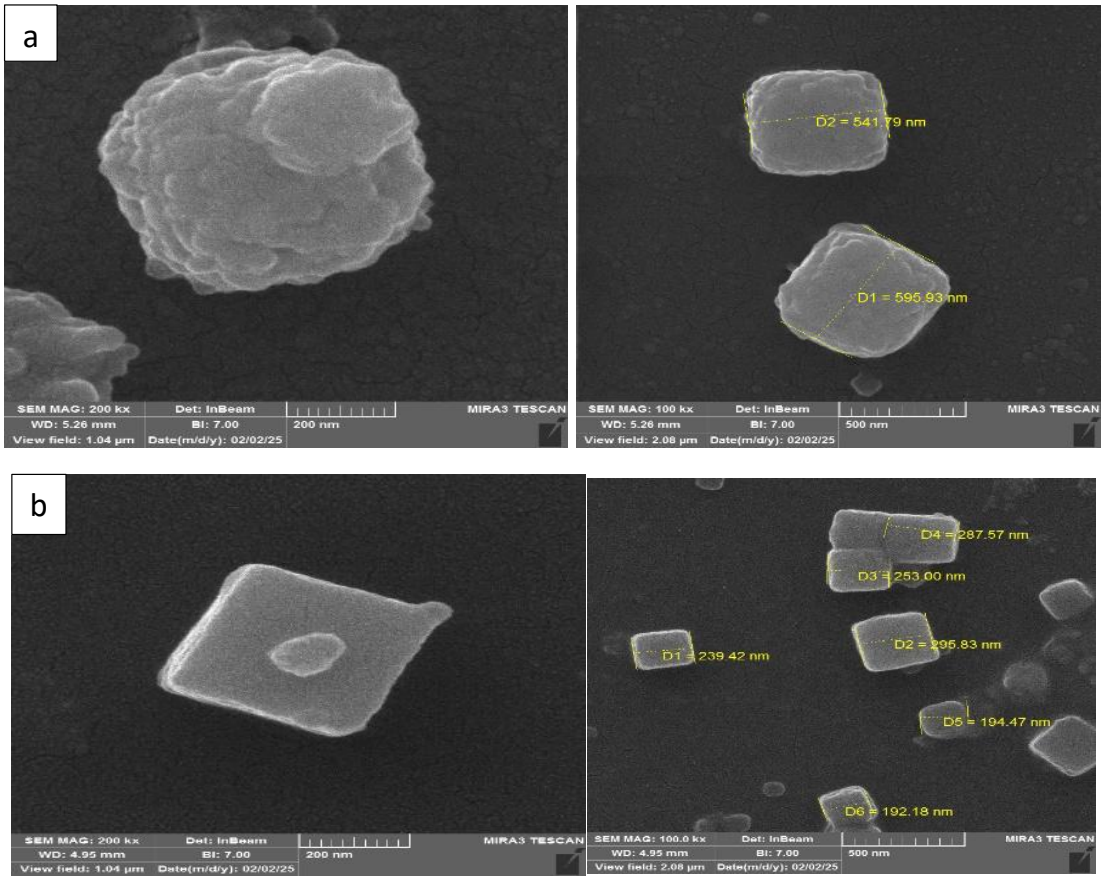

Fig. 5. FE-SEM images and length distribution of Ag NPs measurement at range (200 nm and 500nm): a) 500mJ b)700mJ.

of their attractive forces, NPs aggregated, as seen by the FE-SEM images The FE-SEM images show Zinc Oxide and Silver colloid solutions synthesized by varying laser energy. The homogeneous deposition of (ZnO) coatings, which cover the all substrate in grain clusters-shaped pattern, while the regular aggregation of (Ag) coatings in cubic -shaped pattern, is clear.

Due to the merger of adjacent particles, the particle density increases as the energy of the laser decreases the material a less solid look and more voids. It is important to remember that the resultants of energy 's (Eg) indicate that the optical characteristics of (ZnO and Ag) films may be affected by the merger of nearby particles and the ensuing increases in vacancies.

The FE-SEM images provide important insights into the surface shape of the samples as well as variations in size and particle density of the ZnO and Ag films at (500-700) mJ laser energies [8].

Optical Properties

At various intensities of pulse laser, the optical properties of (ZnO,Ag) colloids solutions at room temperature were studied. UV-Vis spectroscopy was then used to examine the nanostructures' optical properties.

The Absorbance Spectrum (A)

ZnO and Ag NPs' optical absorption spectra at median laser energy (500,700) mJ are shown in Fig. 6. A peak of absorption were seen within wavelength ranges from 200 - 1100 nanometers for PLAL technique. It is evident from test of the absorption spectrum in Fig. 6, that the absorbance of Ag samples increases as the intensity of the laser pulse's increases. This is explained by a higher percentage of ablation, which raises the rate of the particle size. The surface become rougher, increasing the absorption of photon. With increasing wavelength, incoming rays

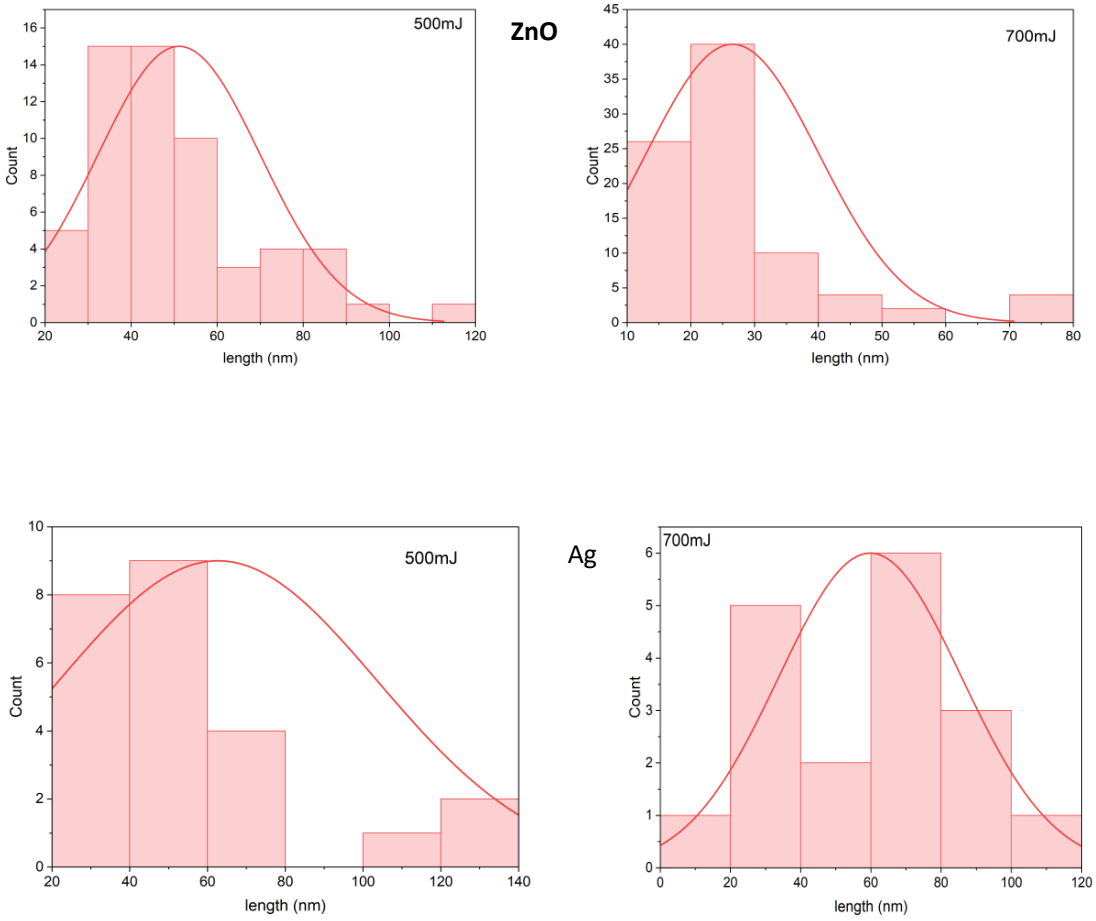

Fig. 6. length distribution of nanoparticles.

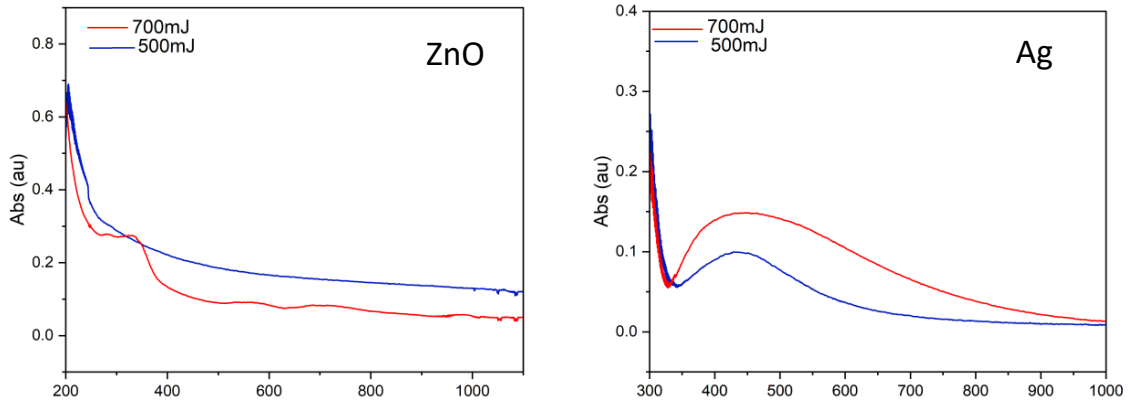

Fig. 7. Absorbance spectra of nanoparticles as a function of wavelength.

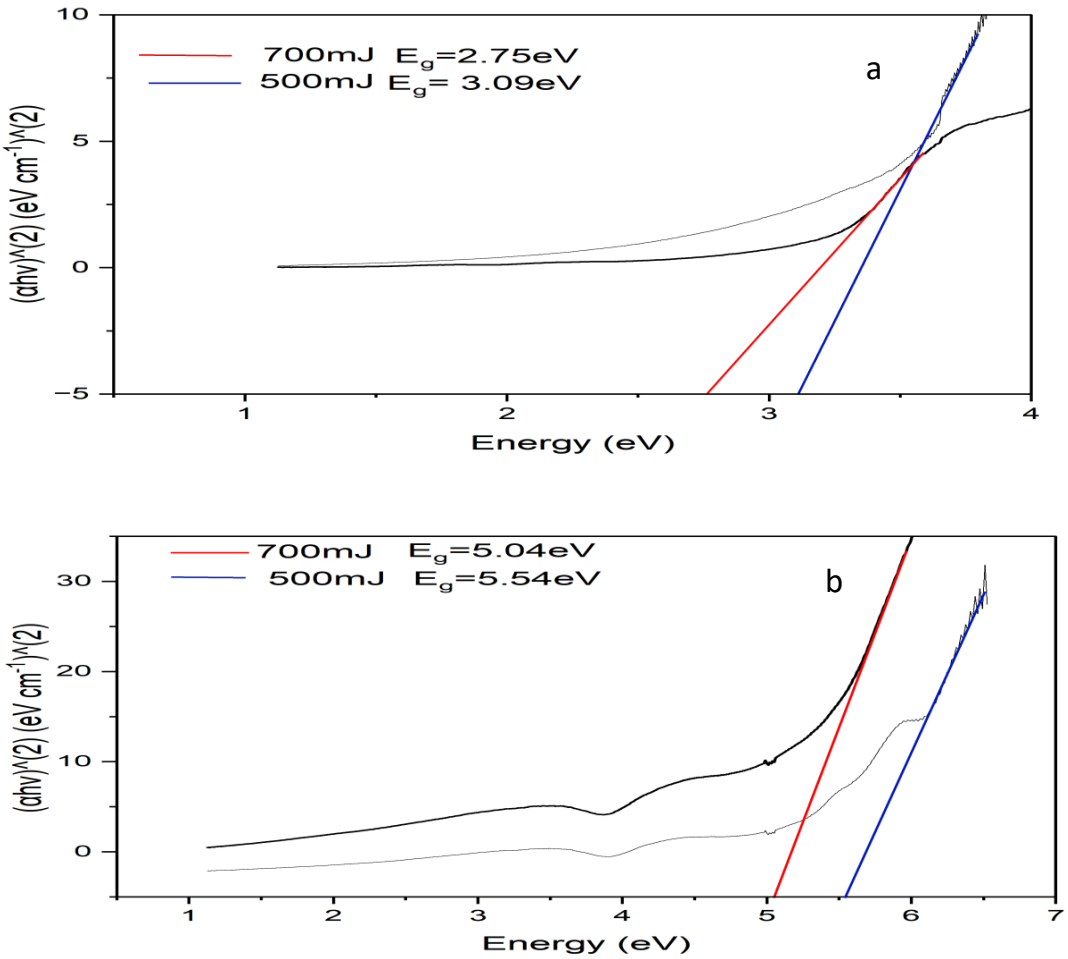

Fig. 8. Energy gap of nanoparticles prepared by PLAL a) ZnO b) Ag.

lose intensity and got fewer able to interact with molecules of solution. As a result, this rays go through mechanisms for the scattering. this relation between roughen particle with absorbance is consistent results' Deepalakshmi K [9]. High absorption at short wavelengths (blue) indicates the formation NPs with smaller size [10].

Energy of Optical Band gap (E_g)

Energy of the optical band gap (E_g), is an important optical constant in semiconductor physics. The suitability of semiconductors for a variety of applications depends on this characteristic [11]. The material's crystal structure impact the value of E_g, giving the impression that specific atom arrangement inside semiconductor affect it extremely [12]. To determine the value of energy gap, one must know the energy of the incoming photon (hv) and the absorption coefficient (α). The band gap energy Eg may be calculated by using the proper formulae:

$$(ahv) = A\,(hv - Eg)^{r} \quad (2)$$

where r=1/2 or 2, Based on the data provided, the E_g values for ZnO and Ag colloid solutions were determine by using Fig. 7 500 and 700 mJ of laser pulse energy were used for the deposition. According to Table 3 resultants of E_g of ZnO decrease from 3.09 to 2.77 eV and 5.54 to 5.04 eV of silver These results are match with [13]. The decrease in band gap energy values with increasing laser pulse energy suggests different particle sizes of ZnO and Ag films. Secondary levels in the band gap, which increase the energy differential, provide an explanation for this result.

As a result, colloid solution has more granules or particles visible. These results are consistent with those that Faiadh [14].

Atomic Absorption Spectroscopy (AAS)

Atomic absorption spectroscopy was used to measure the concentrations of colloidal solutions syntheses by laser ablation in liquid (PLAL), using the device (Analytik jena-Germany). AS follows 10.8, 9.5 ppm (parts per million) of ZnO and 8.3, 3.4 ppm of Ag at 500 mJ and 700mJ, respectively because decreasing particles sizes.

Antibacterial activity

Activity of colloid solutions (ZnO NPs (500), ZnO NPs (700), Ag NPs (500), Ag NPs (700) Were examined by the (M-H) Agar well diffusion experiment opposed to both positive one gram

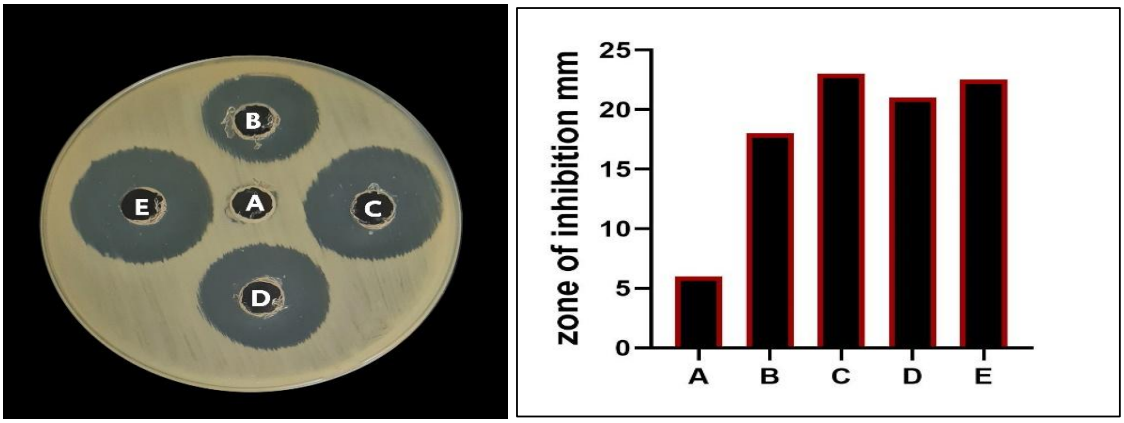

Fig. 9. Antibacterial activity of (Test materials) against *S.aureus.* A, Control. B, (ZnO NPs 500). C, (ZnO NPs 700). D, (Ag NPs 500). E, (Ag NPs 700).

Table 3. The Activity of NPs (Ag ,ZnO).

Kind of bacteria	A	B	C	D	E
S.aureus	6	18	23	21	22.5
E.coli	6	18	20	19	21

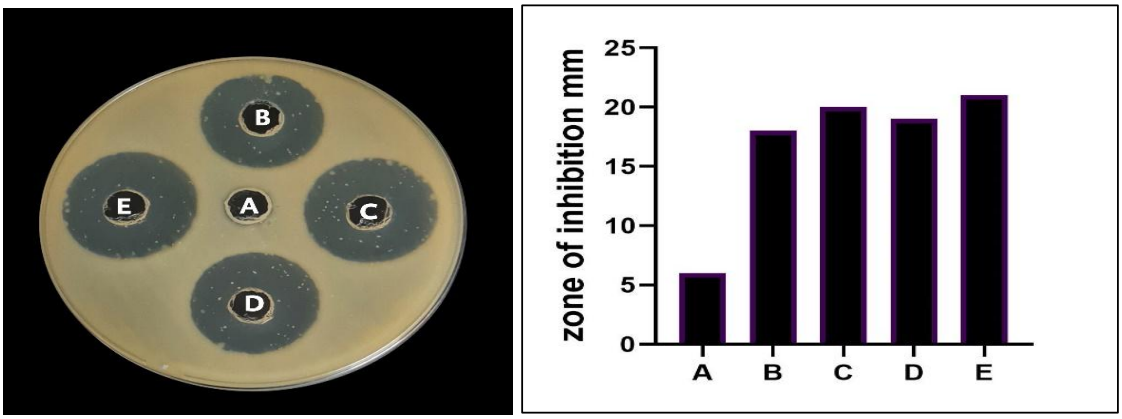

Fig. 10. Antibacterial activity of (Test materials) against E.coli A, Control. B, (ZnO NPs 500). C, (ZnO NPs 700). D, (Ag NPs 500). E, (Ag NPs 700).

Table 4. Comparing between ZnO and Ag nanoparticles syntheses by PLAL at laser energies (500,700) mJ respectively.

	ZnO	Ag
Appropriate laser energy	high	low
Average Crystallite size (nm)	Decrease (14.51- 13.06)	Increase (9.05-22.19)
Diameter mean (nm)	38.81	92.6
Shape	Grain clusters	cubic
Distribution	homogeneous	inhomogeneous
Roughness	less	more
Absorption range (nm)	Begin from 200	Begin from 300
Energy gap (eV)	3.09 – 2.75	5.54 – 5.04
Antibacterial	Equal at 500mJ	Various at 500mJ
	High inhibition	High inhibition
Concentration with laser energy	Less change	More change

and negative one gram species of bacteria [15]. Carefully, (20) milliliters of the agar were transferred into sterilized petri- dishes [16]. A sterile metal wire looping procedure was used to extract the types of bacteria from their own strains [17] by clean tips, wells of six millimeters in diameter were punched into the (M-H)agar-dishes after the microorganisms' cultivation[18]. Various concentrations of the samples were introduced (ZnO NPs (500), ZnO NPs (700), Ag NPs (500), Ag NPs (700) were used. The cultured plates containing the Samples (ZnO NPs (500), ZnO NPs (700), Ag NPs (500), Ag NPs (700)) at 37°C before measuring and recording the average the zones of inhibition diameter [18-20]. The findings of inhibition against the types of bacteria shown in Figs. 7 and 8 and Table 3.

It is observed, that activity of inhibition grow with increasing laser energy for both kinds of the bacteria S.aureus and E.coli because decreasing of grain volumes where it becomes suitable for absorption by the bacteria.

CONCLUSION

By using PLAL with different laser energy at 500 mJ and 700 mJ by 200 pulses, were used to create Ag and ZnO nanostructures using laser- induced plasma. The resultant polycrystalline films cubic structure of Ag and hexagonal structure of ZnO was verified by XRD investigation. Additionally, The aggregation and nanoparticle morphology of Ag nanostructures, which manifested as a cubic-shape and regular aggregation, also grain clusters-shape and homogeneous distribution of ZnO, were demonstrated by the FE-SEM images.Further analysis of the optical characteristics of the Ag nanostructure showed that the band gap energy decreases as laser intensity increases.While antibacterial activity increases with increasing laser energy for both samples (Ag and ZnO). While atomic absorption spectroscopy (AAS) decreases with increasing laser energy especially of Ag.

CONFLICT OF INTEREST

The authors declare that there is no conflict of interests regarding the publication of this manuscript.

REFERENCES

1. Haleem A, Abbas R, Kadhim A. Green Synthesis, Characterization and Antimicrobial Activity of Titanium Dioxide Nanoparticles Using Laser Ablation Technique. Engineering and Technology Journal. 2018;36(1C):11-16.
2. Balachandran A, Sreenilayam SP, Madanan K, Thomas S, Brabazon D. Nanoparticle production via laser ablation synthesis in solution method and printed electronic application - A brief review. Results in Engineering. 2022;16:100646.
3. Khairani IY, Mínguez-Vega G, Doñate-Buendía C, Gökce B. Green nanoparticle synthesis at scale: a perspective on overcoming the limits of pulsed laser ablation in liquids for high-throughput production. Physical Chemistry Chemical Physics. 2023;25(29):19380-19408.
4. Lam J, Amans D, Chaput F, Diouf M, Ledoux G, Mary N, et al. γ-Al_2O_3 nanoparticles synthesised by pulsed laser ablation in liquids: a plasma analysis. Phys Chem Chem Phys. 2014;16(3):963-973.
5. Alheshibri M, Kotb E, A.Haladu S, Al Baroot A, Drmosh QA, Ercan F, et al. Synthesis of highly stable Ag/Ta_2O_5 nanocomposite by pulsed laser ablation as an effectual antibacterial agent. Optics and Laser Technology. 2023;162:109295.
6. Bhattacharya D. Plasma dynamics from laser ablated solid lithium. Pramana. 2000;55(5-6):823-833.
7. Abbas IK, Aadim KA. Synthesis and Study of Structural Properties of Calcium Oxide Nanoparticles Produced by Laser-Induced Plasma and its Effect on Antibacterial Activity. Science and Technology Indonesia. 2022;7(4):427-434.
8. Indirajith R, Rajalakshmi M, Ramamurthi K, Ahamed MB, Gopalakrishnan R. Synthesis of ZnSe Nano Particles, Deposition of ZnSe Thin Films by Electron Beam Evaporation and Their Characterization. Ferroelectrics. 2014;467(1):13-21.
9. Khodorov A, Gomes MJM. Preparation and optical characterization of lanthanum modified lead zirconate titanate thin films on indium-doped tin oxide-coated glass substrate. Thin Solid Films. 2006;515(4):1782-1787.
10. Naser DK, Abbas AK, Aadim KA. Zeta Potential of Ag, Cu, ZnO, CdO and Sn Nanoparticles Prepared by Pulse Laser Ablation in Liquid Environment. Iraqi Journal of Science. 2020:2570-2581.
11. Zheng BJ, Lian JS, Zhao L, Jiang Q. Optical and electrical properties of Sn-doped CdO thin films obtained by pulse laser deposition. Vacuum. 2011;85(9):861-865.
12. Fattahi B, Mahdieh MH. Effect of inter-pulse delay time on production and size properties of colloidal nanoparticles prepared by collinear double-pulse laser ablation in liquid. Laser Physics Letters. 2016;13(8):086101.
13. Zakaria MA, Menazea AA, Mostafa AM, Al-Ashkar EA. Ultra-thin silver nanoparticles film prepared via pulsed laser deposition: Synthesis, characterization, and its catalytic activity on reduction of 4-nitrophenol. Surfaces and Interfaces. 2020;19:100438.
14. Ahmed AF, Mutlak FAH, Abbas QA. Evaluation of cold plasma effect to achieve fullerene and zinc oxide-fullerene hydrophobic thin films. Appl Phys A. 2022;128(2).
15. Bahjat HH, Ismail RA, Sulaiman GM, Jabir MS. Magnetic Field-Assisted Laser Ablation of Titanium Dioxide Nanoparticles in Water for Anti-Bacterial Applications. Journal of Inorganic and Organometallic Polymers and Materials. 2021;31(9):3649-3656.
16. Khashan KS, Abdulameer FA, Jabir MS, Hadi AA, Sulaiman GM. Anticancer activity and toxicity of carbon nanoparticles produced by pulsed laser ablation of graphite in water. Advances in Natural Sciences: Nanoscience and Nanotechnology. 2020;11(3):035010.
17. The Effect of Metal Nanoparticle on LH, FSH and Testosterone in Male Rats. Indian Journal of Public Health Research and Development. 2020.
18. Mohammed MKA, Mohammad MR, Jabir MS, Ahmed DS. Functionalization, characterization, and antibacterial activity of single wall and multi wall carbon nanotubes. IOP Conference Series: Materials Science and Engineering. 2020;757(1):012028.
19. Jihad MA, Noori FTM, Jabir MS, Albukhaty S, AlMalki FA, Alyamani AA. Polyethylene Glycol Functionalized Graphene Oxide Nanoparticles Loaded with Nigella sativa Extract: A Smart Antibacterial Therapeutic Drug Delivery System. Molecules. 2021;26(11):3067.
20. Thamer AA, Noor hussein M, Hashim Imran S, Hassani RH. Sol-Gel Process Optimization for CuO Nanoparticle Synthesis Achieving High Purity and Homogeneity. Journal of Physics: Conference Series. 2025;2974(1):012019.